Search for Solar Axions via Axion-Photon Coupling with the Majorana Demonstrator

I. J. Arnquist, F. T. Avignone III, A. S. Barabash, C. J. Barton, K. H. Bhimani, E. Blalock, B. Bos, M. Busch, M. Buuck, T. S. Caldwell, Y. Y. D. Chan, C. D. Christofferson, P.-H. Chu, M. L. Clark, C. C. Cuesta, L. A. Detwiler, U. W. Efremenko, S. H. Ejiri, S. R. Elliott, G. K. Giovanetti, M. P. Green, S. J. Gruszko, C. T. S. Guinn, K. V. E. Guiseppe, C. R. Haufe, R. Henning, D. Hervas Aguilar, L. W. Hoppe, A. Hostiuc, M. F. Kidd, R. T. Kouzes, T. E. Lannen V., A. Li, A. M. Lopez, L. M. López-Castaño, E. L. Martin, R. D. Martin, R. Massarczyk, S. J. Meijer, A. K. Oli, G. Othman, A. M. Lopez, D. Pettus, L. S. Paudel, W. P. Poon, L. C. Radford, A. L. Reine, K. Rielage, N. W. Ruof, D. C. Schaper, D. Tedeschi, R. L. Varner, S. Vasilyev, L. F. Wilkerson, K. C. Wiseman, U. Xu, A. Xu, A. S. C.-H. Yu, and B. X. Zhu, S. Pauls, R. Zhu, L. Varner, A. Vasilyev, L. F. Wilkerson, L. Wiseman, L. W. Ruof, L. Varner, S. Vasilyev, L. F. Wilkerson, S. Vasilyev, L. S. Paudel, R. L. Varner, L. Varner, S. Vasilyev, L. F. Wilkerson, R. C. Wiseman, M. Xu, Ruof, S. C.-H. Yu, A. And B. X. Zhu, R. Zhu, R. L. Varner, R. C. Wiseman, L. Varner, S. Vasilyev, L. F. Wilkerson, R. C. Wiseman, L. Varner, R. C.-H. Yu, A. A. Reine, R. C.-H. Yu, A. A. Reine, R. C.-H. Yu, A. Reine, R. C.-H. Yu, A. A. Reine, R. C.-H. Yu, A. A. A. Reine, R. A. A. Yu, A. A. Yu, A.

(MAJORANA Collaboration)

¹Pacific Northwest National Laboratory, Richland, Washington 99354, USA ²Department of Physics and Astronomy, University of South Carolina, Columbia, South Carolina 29208, USA ³Oak Ridge National Laboratory, Oak Ridge, Tennessee 37830, USA ⁴National Research Center "Kurchatov Institute" Institute for Theoretical and Experimental Physics, Moscow, 117218 Russia ⁵Department of Physics, University of South Dakota, Vermillion, South Dakota 57069, USA ⁶Department of Physics and Astronomy, University of North Carolina, Chapel Hill, North Carolina 27514, USA 7 Triangle Universities Nuclear Laboratory, Durham, North Carolina 27708, USA ⁸Department of Physics, North Carolina State University, Raleigh, North Carolina 27695, USA ⁹Department of Physics, Duke University, Durham, North Carolina 27708, USA ¹⁰Center for Experimental Nuclear Physics and Astrophysics, and Department of Physics, University of Washington, Seattle, Washington 98195, USA ¹¹Nuclear Science Division, Lawrence Berkeley National Laboratory, Berkeley, California 94720, USA ¹²South Dakota Mines, Rapid City, South Dakota 57701, USA ¹³Los Alamos National Laboratory, Los Alamos, New Mexico 87545, USA ¹⁴Centro de Investigaciones Energéticas, Medioambientales y Tecnológicas, CIEMAT 28040, Madrid, Spain ¹⁵Department of Physics and Astronomy, University of Tennessee, Knoxville, Tennessee 37916, USA ⁶Research Center for Nuclear Physics, Osaka University, Ibaraki, Osaka 567-0047, Japan ¹⁷Physics Department, Williams College, Williamstown, Massachusetts 01267, USA ¹⁸Tennessee Tech University, Cookeville, Tennessee 38505, USA ¹⁹Department of Physics, Engineering Physics and Astronomy, Queen's University, Kingston, Ontario K7L 3N6, Canada ²⁰Department of Physics, Indiana University, Bloomington, Indiana 47405, USA ²¹IU Center for Exploration of Energy and Matter, Bloomington, Indiana 47408, USA ²²Joint Institute for Nuclear Research, Dubna, 141980 Russia

(Received 13 June 2022; accepted 21 July 2022; published 19 August 2022)

Axions were originally proposed to explain the strong-CP problem in QCD. Through axion-photon coupling, the Sun could be a major source of axions, which could be measured in solid state detection experiments with enhancements due to coherent Primakoff-Bragg scattering. The MAJORANA DEMONSTRATOR experiment has searched for solar axions with a set of ⁷⁶Ge-enriched high purity germanium detectors using a 33 kg-yr exposure collected between January, 2017 and November, 2019. A temporal-energy analysis gives a new limit on the axion-photon coupling as $g_{a\gamma} < 1.45 \times 10^{-9} \ {\rm GeV^{-1}}$ (95% confidence level) for axions with mass up to $100 \ {\rm eV}/c^2$. This improves laboratory-based limits between about $1 \ {\rm eV}/c^2$ and $100 \ {\rm eV}/c^2$.

DOI: 10.1103/PhysRevLett.129.081803

Published by the American Physical Society under the terms of the Creative Commons Attribution 4.0 International license. Further distribution of this work must maintain attribution to the author(s) and the published article's title, journal citation, and DOI. Axions were originally motivated as the Peccei-Quinn solution to the strong-charge parity (*CP*) problem in quantum chromodynamics (QCD) [1–5], where a *CP*-violating parameter in the strong force is heavily constrained by neutron electric dipole moment

measurements [6-8]. Axion models have evolved from the original QCD axion characterized by a constrained relationship between mass and coupling constant to a group of pseudoscalar particles beyond the standard model (SM), called axionlike particles (ALPs). Axions and ALPs are dark matter candidates [9–11] and can serve as a portal to the dark sector [12], and they motivate active global searches with a comprehensive range of techniques [7,13–16]. Axions can couple to photons directly and via neutral pions, so the axion-photon coupling g_{av} is typically nonzero [17]. In the Kim-Shifman-Vainshtein-Zakharov (KSVZ) generic hadronic model [18,19], axions are considered "invisible," with no tree-level axion-electron coupling g_{ae} ; however, KSVZ axions couple to photons as expressed in Eq. (1), where N and E are the dimensionless coefficients for color and electromagnetic anomalies. A window of $0.25 \le |E/N - 1.92| \le 12.75$ has been determined for realistic QCD KSVZ axions [20].

$$g_{a\gamma} = \frac{m_a}{\text{eV}} \frac{2.0}{10^{10} \text{ GeV}} \left(\frac{E}{N} - 1.92\right)$$
 (1)

The axion-photon coupling $g_{a\gamma}$ in electromagnetic fields enables the Primakoff effect [21], where axions can convert into photons, and its inverse process. Astrophysical and cosmological measurements such as stellar cooling rates have set stringent limits on $g_{a\gamma}$ [7,22–24]. A recent analysis of horizontal branch (HB) stars in a sample of 39 galactic globular clusters gives the limit $g_{a\gamma} < 0.66 \times 10^{-10} \text{ GeV}^{-1}$ at a 95% confidence level (CL), one of the strongest constraints to date in a wide mass range [25]. Complementary to these observations, laboratory-based axion searches provide valuable independent tests with a variety of physics and experimental techniques [15–17,26], probing a large phase space of QCD models.

The Sun may be a major source of axions [23,27–30], producing axions by Primakoff scattering of thermal photons in the electromagnetic field of the solar plasma (the inverse Primakoff effect) [22–24]. A modern parameterization of the solar axion flux from the Primakoff process is given by Eq. (2), where E_a is the axion energy in keV, $\lambda \equiv (g_{a\gamma} \times 10^8 \text{ GeV})^4$, and $\Phi_0 \equiv 6.02 \times 10^{14} \text{ cm}^{-2} \text{ sec}^{-1} \text{ keV}^{-1}$ [26,31–33].

$$\frac{d\Phi}{dE_a} = \sqrt{\lambda} \Phi_0 E_a^{2.481} e^{-E_a/1.205} \tag{2}$$

In the presence of strong magnetic fields, solar axions can be converted to electromagnetic signals. This mechanism, the Primakoff effect, is the one used on Earth by axion helioscope experiments. The CERN Axion Solar Telescope (CAST) experiment tracks solar axions over a wide range of mass using a dipole magnet originally built for the Large Hadron Collider and its best limit is similar to HB limits for $m_a \lesssim 0.02 \text{ eV}/c^2$ [31,33,34]. However, the

CAST experiment quickly loses its sensitivity at the threshold of $m_a \sim 1.2 \text{ eV}/c^2$, where solid state detectors may begin to play a significant role.

As solar axions reach detector materials, they may also convert into photons by the intense local electric field of the target atomic nucleus. High Purity Germanium (HPGe) detectors and other solid state detectors may enjoy a great enhancement to these axion-induced photon signals when the condition of coherent Bragg diffraction is satisfied. The Bragg condition correlates photon energies E with axion incident angles in respect to crystalline planes of the detectors, producing a strong dependence of the axion-photon conversion probability on the Sun's position at a given time t and the crystal plane orientation. This is a unique signature of solar axions with both time- and energy-dependent features [35–37].

Pioneered by the SOLAX [38] experiment, a series of solid state experiments probed $g_{a\gamma}$ using this coherent Primakoff-Bragg scattering technique [38–42]. The current best limits of these experiments, $g_{a\gamma} < 1.7 \times 10^{-9} \text{ GeV}^{-1}$ at 90% CL and $g_{a\gamma} < 2.15 \times 10^{-9} \text{ GeV}^{-1}$ at 95% CL, were established by DAMA NaI detectors [39] and EDELWEISS-II germanium detectors [42], respectively. As the photon energies are assumed to be the same as the kinetic energies of incident axions, these limits are valid for an axion mass from near zero up to $100 \text{ eV}/c^2$, where the mass energy of axions begins to yield a non-negligible energy correction.

The [001] axis of a Ge crystal is determined by the crystal boule axis, which corresponds to the vertical direction in most experiments, and only the horizontal orientation of the crystal planes (the azimuthal angle ϕ) needs to be measured to predict solar axion signatures at a given time. This approach was used by CDMS for their germanium detectors with a few-degree precision [41]. Predictions for the energy-and time-dependent signals from coherent Primakoff-Bragg axion signatures were given in Refs. [38,43,44] and explored specifically for HPGe detectors at the location of the Sanford Underground Research Facility (SURF) in Lead, South Dakota, in Ref. [45].

If crystal horizontal orientations are unknown, the lack of information leads to reduced sensitivity, but the Primakoff-Bragg technique can still be exploited. The angle-dependent signal rate $R(\phi,E,t)$ can be averaged over all possible crystal horizontal orientations to give an angle-averaged signal rate $\bar{R}(E,t)$ in the entire experiment, as $\bar{R}(E,t) = \int_{-\pi/4}^{\pi/4} R(\phi,E,t) d\phi/(\pi/2)$. This angle averaging approach was first used for the DAMA best limit [39]. Within the Bayesian framework, the angle-averaging approach is the key step of marginalization over the nuisance parameter of crystal horizontal orientation. The prior for this nuisance parameter is uniform, if only the crystal boule axis is known. The angle-averaged signal rate still has strong time and energy dependence, as shown in Fig. 1, but it is not as distinct as those for specific crystal

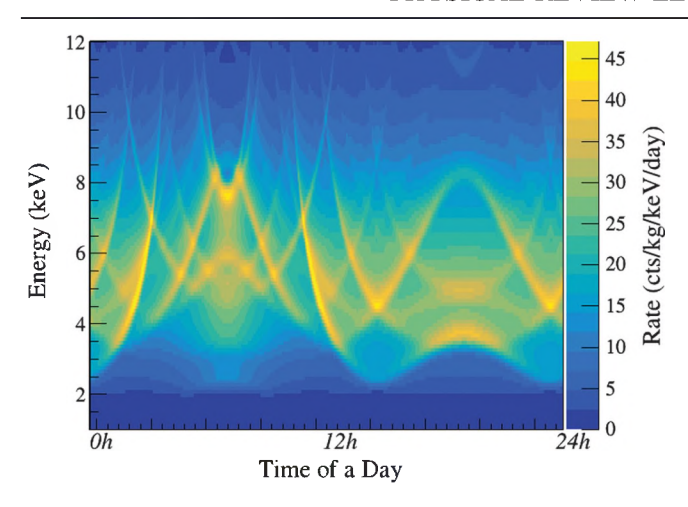


FIG. 1. Axion signatures from coherent Primakoff-Bragg scattering averaged over all possible orientations of horizontal crystal planes, predicted for a 1-kg HPGe detector located at SURF for $g_{a\gamma}=10^{-8}~{\rm GeV^{-1}}$. The time duration shown is a full day.

horizontal orientations, examples of which can be found in Refs. [41,42,45]. The reduction of sensitivity was found to be approximately a factor of 4 for λ [45], which is about 40% for g_{ay} .

The MAJORANA DEMONSTRATOR experiment, located on the 4850' level at SURF [46], searched for neutrinoless double beta $(0\nu\beta\beta)$ decay in ⁷⁶Ge with 44 kg of p-type, point-contact HPGe detectors, of which 30 kg were enriched in ⁷⁶Ge [47,48]. MAJORANA detectors were deployed in two separate modules that were shielded against environmental radioactivity by layers of compact lead and copper shielding. The DEMONSTRATOR used extensive material screening and stringent cleanliness measures to achieve exceedingly low background. Surface exposure of the enrGe detectors was carefully limited, resulting in significantly lower background at low energy than the ^{nat}Ge detectors. The DEMONSTRATOR module 1 detectors started data taking in 2015, and module 2 became online in late 2016. Low energy physics was enabled by DEMONSTRATOR low-noise electronics [49], and this analysis uses low-noise physics data taken between January, 2017 and November, 2019 by more than 20 enrGe detectors, with a background of about 0.05 counts/(keV kg d) at 5 keV. MAJORANA HPGe detectors have excellent energy resolution that is approaching 0.1% full-width at half maximum at the 2039 keV Q value of the $0\nu\beta\beta$ decay [48], the best among all $0\nu\beta\beta$ experiments. The 1- σ energy resolution is better than 0.2 keV in the 5 to 22 keV energy range used in this analysis.

HPGe detectors are known to have a transition layer immediately beneath the surface dead layer. [50]. Charge carriers diffuse out of the transition layer slowly, resulting in pulses with slower rise time and degraded energy. A novel data analysis method was recently developed to reject these slow pulses at low energy in the DEMONSTRATOR [51,52]. After denoising using a wavelet packet transform

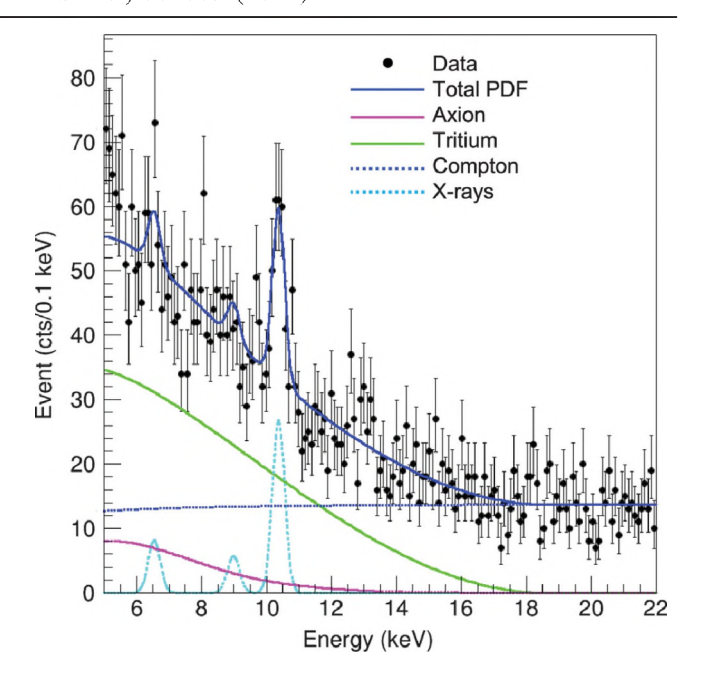


FIG. 2. The energy spectrum of low energy events (Data), shown along with the best fit of the extended composite model (Total PDF) and individual components. All components have the energy efficiency folded.

and a Daubechies-2 wavelet function, each low energy waveform is fitted with a heuristic exponentially modified Gaussian that generically resembles the waveform and features an effective slowness parameter corresponding to the slope of the pulse rising edge. A cut is placed on the slowness parameter to accept fast waveforms only. The cut efficiency is calculated based on forward Compton scattering of 239-keV photons from routine ²²⁸Th source calibrations. By requiring the total energy to be shared in exactly two HPGe detectors, a sample dominated by real 239-keV photon events is obtained, which is made of bulk events since events with slow pulses do not have sum energy lying in the 239-keV peak due to energy degradation. Within this sample, detector hits with lower energy can be used to calculate the total cut efficiency, which is close to 90% above 5 keV [53]. A paper with details on data selection, data cleaning, and analysis cuts used in low energy analysis of the DEMONSTRATOR is in preparation. To avoid lower efficiency and associated large relative uncertainties below 5 keV, this solar axion analysis starts at 5 keV and ends at 22 keV, which is beyond the 18.6-keV end point of tritium β decay. The energy spectrum of the low energy events is shown in Fig. 2.

The data analysis has two steps. First, a maximum likelihood analysis was carried out to fit the data with a composite model with both axion signals and background components. Then, a Bayesian analysis was performed to extract an exclusion limit on axions. Because of the lack of knowledge on the horizontal crystal plane angles for individual detectors, the angle-averaged Primakoff-Bragg

axion signature $\bar{R}(E,t)$ is used to construct the signal model in both energy and temporal dimensions. The position of the Sun between January, 2017 and November, 2019 is tracked using the Naval Observatory Vector Astrometry Software (NOVAS) [54], and the axion probability density function (PDF) is evaluated over the three-year period with five-minute precision. The background PDFs include the tritium β decay, a flat background representing an extrapolation of the Compton continuum of photons at higher energy, and three Gaussian peaks representing the x rays of cosmogenic ⁵⁵Fe (6.54 keV), ⁶⁵Zn (8.98 keV), and ⁶⁸Ge (10.37 keV). Since tritium, ⁵⁵Fe, ⁶⁵Zn, and ⁶⁸Ge were generated during limited surface exposure, they are modeled to decay away with corresponding halflives, while the Compton continuum is constant in time. Both background and signal PDFs are weighted by the time-dependent exposure, which is the product of datataking live time and active mass, and folded with the total cut efficiency in energy. A composite model is constructed by multiplying the PDF (\mathcal{P}) of the individual components with the corresponding strength (n) and adding them together, as expressed in Eq. (3),

$$\mathcal{P}_{\text{tot}}(\vec{x}; \vec{n}) = n_a \mathcal{P}_a(\vec{x}) + n_C \mathcal{P}_C(\vec{x}) + n_T \mathcal{P}_T(\vec{x}) + \sum_{i=1}^{n_{\text{pks}}} n_i \mathcal{P}_i(\vec{x})$$
(3)

where $\vec{x} = (E, t)$ and a, C, T, i indicate axions, Compton scatters, tritium, and the three x-ray peaks, respectively. The free parameters (\vec{n}) are the strengths of axion and backgrounds. Each individual PDF on the right side of Eq. (3) is normalized to 1, so that the added total probability is normalized to the total number of events n_D detected in the data.

$$\int \mathcal{P}_{\rm tot}(\vec{x}; \vec{n}) d\vec{x} = n_a + n_C + n_T + \sum_{i=1}^{n_{\rm pks}} n_i = n_D \quad (4)$$

Events from enriched detectors are combined together to form a single cohort and fitted with the composite model in an unbinned extended maximum likelihood method using the ROOFIT plus ROOSTATS package [55] in root ver. 6.22/06 [56], the result of which is shown in Fig. 2. The number of axions is fitted to be $n_a = 297 \pm 138$, which is consistent with zero at 2.2σ .

Reference [45] pointed out that, when the angle averaged axion PDF is used, good statistical behaviors including the applicability of Wilks' theorem [57] is guaranteed only for experiments with a dozen or more detectors. Otherwise, statistical sampling, such as frequentist test statistic sampling as done by EDELWEISS [42] or Bayesian posterior sampling as in this analysis, will be necessary to correctly evaluate the statistical penalty of the information loss on the crystalline orientation. Since there are 20 or more detectors in this analysis, good statistical behavior is

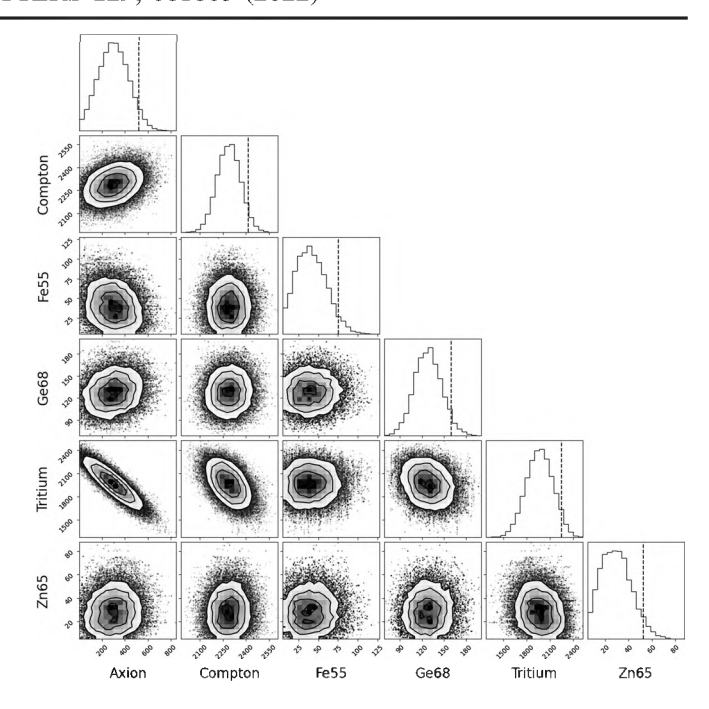


FIG. 3. Contours for pairs of parameters in the RooStats MCMC sampling, and the projected posterior distributions for each parameter. Each vertical line in the posterior distributions indicates a 95% interval.

guaranteed [45] and an estimation of a frequentist 95% limit on n_a can be approximated as the best-fit plus $1.65\sigma = 297 + 1.65 \times 138 = 525$. A Bayesian analysis based on Markov-Chain Monte Carlo (MCMC) sampling was carried out for accurate limit setting. The Metropolis-Hastings (MH) sampling algorithm in ROOSTATS is utilized to construct the MCMC chains with five million iterations. The axion number n_a is the parameter of interest, and the rest of \vec{n} are nuisance parameters. The other nuisance parameter ϕ was already marginalized in $\bar{R}(E,t)$. A uniform prior between 0 and all events in the analyzed datasets is used for n_a , similar to the CDMS analysis [41]. Posterior probability distributions after sampling are shown in Fig. 3, along with correlations among parameters. The median values in the Bayesian posteriors match well with their corresponding maximumlikelihood best fits. n_a is found to be less than 519 at a 95% CL. This 95% Bayesian upper limit on n_a is close to the approximate frequentist limit and it translates to $\lambda < 4.48 \times$ 10^{-4} or $g_{ay} < 1.45 \times 10^{-9}$ GeV⁻¹, improving on the limits from DAMA (90% CL) and EDELWEISS-II (95% CL).

Systematic uncertainties arise from cut efficiency and energy. The dominant contribution is cut efficiency, where lower efficiency leads to a worse limit and vice versa. By varying the cut efficiency within its own uncertainties [53], a change of up to 16% is found on the limit of λ . Based on the cosmogenic x-ray peaks at low energy, the energy scale is found to be accurate to within 0.1 keV of the expected values [53,58]. An energy scale uncertainty of ± 0.1 keV introduces a 6% uncertainty in the limit. The variation of energy

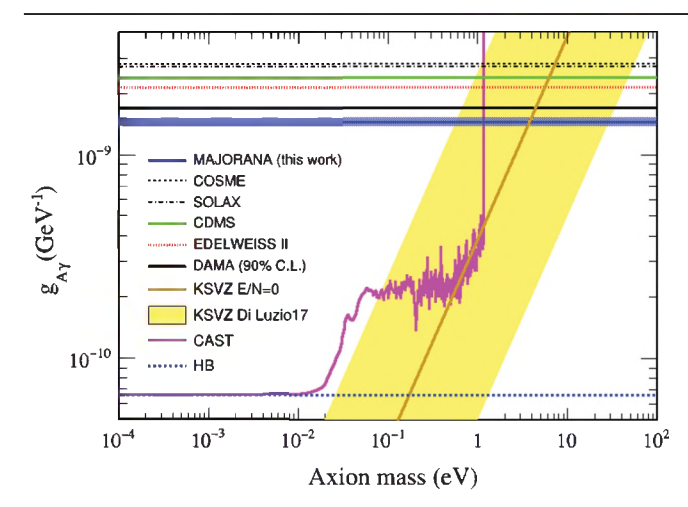


FIG. 4. g_{ay} limit obtained in this analysis (solid blue line), with the uncertainty shown as a band around the limit. The HB constraints [25], the CAST limits [31,33,34,63], and other solid state limits are also shown for SOLAX [38], DAMA [39], COSME [40], CDMS [41] and EDELWEISS-II [42]. All limits are for 95% CL, except for the 90% DAMA limit. The KSVZ axion phase space is shown with the realistic range of E/N found in [20].

resolution throughout time yields another 5% uncertainty. In total, an 18% systematic uncertainty is associated with the limit on λ , which is a 5% uncertainty on g_{ay} .

In conclusion, a temporal-energy analysis was performed by the Majorana Demonstrator experiment to search for coherent Primakoff-Bragg axion signals between 5 and 22 keV with a total exposure of 33 kg-yr, the rate of which is found to be consistent with zero. A new limit of 95% CL on the axion-photon coupling is obtained as $g_{a\gamma} < 1.45 \times$ 10⁻⁹ GeV⁻¹ in a Bayesian approach. This improves the limit in laboratory searches for axion mass between $1.2 \text{ eV}/c^2$ and $100 \text{ eV}/c^2$, as shown in Fig. 4, and it continues to exclude KSVZ axions in the larger phase space. An intriguing excess of events was observed by the XENON1T experiment at 1-5 keV [59], which could be due to tritium background or a number of new physics signals. Examining the XENON1T excess against the solar axion hypothesis leads to a range of theoretical considerations [60-62]. The limit established in this Letter is not sensitive enough to exclude the possibility of the XENON1T excess being Primakoff solar axions.

This Letter presented here by the DEMONSTRATOR is one important step forward to improve the best limit in a long series of experimental efforts of using solid-state detectors to effectively probe the $1 \text{ eV}/c^2$ to $100 \text{ eV}/c^2$ mass range, more than twenty years after the DAMA best limit was published. The analysis method used here can be readily employed by the ton-scale Large Enriched Germanium Experiment for Neutrinoless $\beta\beta$ Decay (LEGEND) [64]. With a 10 ton-year exposure and lower background than the DEMONSTRATOR, LEGEND has the potential to effectively probe g_{ay} well below 10^{-9} GeV⁻¹

without measuring the crystal orientations of hundreds of individual detectors.

This material is based upon work supported by the U.S. Department of Energy, Office of Science, Office of Nuclear Physics under Contracts or Awards No. DE-AC02-05CH11231, No. DE-AC05-00OR22725, No. DE-AC05-76RL0130, No. DE-FG02-97ER41020, No. DE-FG02-97ER41033, No. DE-FG02-97ER41041, No. SC0012612, No. DE-SC0014445, No. DE-SC0018060, and No. LANLEM77/LANLEM78. We acknowledge support from the Particle Astrophysics Program and Nuclear Physics Program of the National Science Foundation through Grants No. MRI-0923142, No. PHY-1003399, No. PHY-1102292, No. PHY-1206314, No. PHY-1614611, No. PHY-1812409, No. PHY-1812356, and No. PHY-2111140. We gratefully acknowledge the support of the Laboratory Directed Research & Development (LDRD) program at Lawrence Berkeley National Laboratory for this work. We gratefully acknowledge the support of the U.S. Department of Energy through the Los Alamos National Laboratory LDRD Program and through the Pacific Northwest National Laboratory LDRD Program for this work. We gratefully acknowledge the support of the South Dakota Board of Regents Competitive Research Grant. We acknowledge the support of the Natural Sciences and Engineering Research Council of Canada, funding reference number SAPIN-2017-00023, and from the Canada Foundation for Innovation John R. Evans Leaders Fund. This research used resources provided by the Oak Ridge Leadership Computing Facility at Oak Ridge National Laboratory and by the National Energy Research Scientific Computing Center, a U.S. Department of Energy Office of Science User Facility located at Lawrence Berkeley National Laboratory. We thank our hosts and colleagues at the Sanford Underground Research Facility for their support.

^{*}Present address: SLAC National Accelerator Laboratory, Menlo Park, California 94025, USA.

[†]Present address: Duke University, Durham, North Carolina 27708, USA.

[‡]Present address: Universität Hamburg, Institut für Experimentalphysik, Hamburg, Germany.

[§]wenqin.xu@usd.edu

xiaoyu.x.zhu@jpl.nasa.gov

^{**}Present address: Jet Propulsion Laboratory, California Institute of Technology, Pasadena, California 91109, USA.

^[1] R. D. Peccei and H. R. Quinn, CP Conservation in the Presence of Pseudoparticles, Phys. Rev. Lett. 38, 1440 (1977).

^[2] R. D. Peccei and H. R. Quinn, Constraints imposed by CP conservation in the presence of pseudoparticles, Phys. Rev. D 16, 1791 (1977).

^[3] S. Weinberg, A New Light Boson?, Phys. Rev. Lett. **40**, 223 (1978).

- [4] F. Wilczek, Problem of Strong P and T Invariance in the Presence of Instantons, Phys. Rev. Lett. **40**, 279 (1978).
- [5] R. D. Peccei, The strong CP problem and axions, Lect. Notes Phys. **741**, 3 (2008).
- [6] C. A. Baker, D. D. Doyle, P. Geltenbort, K. Green, M. G. D. van der Grinten, P. G. Harris, P. Iaydjiev, S. N. Ivanov, D. J. R. May, J. M. Pendlebury, J. D. Richardson, D. Shiers, and K. F. Smith, Improved Experimental Limit on the Electric Dipole Moment of the Neutron, Phys. Rev. Lett. 97, 131801 (2006).
- [7] J. E. Kim and G. Carosi, Axions and the strong CP problem, Rev. Mod. Phys. **82**, 557 (2010).
- [8] J. M. Pendlebury *et al.*, Revised experimental upper limit on the electric dipole moment of the neutron, Phys. Rev. D 92, 092003 (2015).
- [9] J. Preskill, M. B. Wise, and F. Wilczek, Cosmology of the invisible axion, Phys. Lett. 120B, 127 (1983).
- [10] L. F. Abbott and P. Sikivie, A cosmological bound on the invisible axion, Phys. Lett. 120B, 133 (1983).
- [11] M. Dine and W. Fischler, The not-so-harmless axion, Phys. Lett. **120B**, 137 (1983).
- [12] R. Essig et al., Dark sectors and new, light, weakly-coupled particles, arXiv:1311.0029.
- [13] W. Buchmüller, R. D. Peccei, and T. Yanagida, Leptogenesis as the origin of matter, Annu. Rev. Nucl. Part. Sci. 55, 311 (2005).
- [14] L. J. Rosenberg, Dark-matter QCD-axion searches, Proc. Natl. Acad. Sci. U.S.A. 112, 12278 (2015).
- [15] P. W. Graham, I. G. Irastorza, S. K. Lamoreaux, A. Lindner, and K. A. van Bibber, Experimental searches for the axion and axion-like particles, Annu. Rev. Nucl. Part. Sci. 65, 485 (2015).
- [16] I. G. Irastorza and J. Redondo, New experimental approaches in the search for axion-like particles, Prog. Part. Nucl. Phys. 102, 89 (2018).
- [17] P. Sikivie, Invisible axion search methods, Rev. Mod. Phys. 93, 015004 (2021).
- [18] J. E. Kim, Weak-Interaction Singlet and Strong CP Invariance, Phys. Rev. Lett. 43, 103 (1979).
- [19] M. A. Shifman, A. I. Vainshtein, and V. I. Zakharov, Can confinement ensure natural CP invariance of strong interactions?, Nucl. Phys. B166, 493 (1980).
- [20] L. Di Luzio, F. Mescia, and E. Nardi, Redefining the Axion Window, Phys. Rev. Lett. 118, 031801 (2017).
- [21] H. Primakoff, Photo-production of neutral mesons in nuclear electric fields and the mean life of the neutral meson, Phys. Rev. **81**, 899 (1951).
- [22] D. A. Dicus, E. W. Kolb, V. L. Teplitz, and R. V. Wagoner, Astrophysical bounds on the masses of axions and Higgs particles, Phys. Rev. D 18, 1829 (1978).
- [23] G. G. Raffelt, Astrophysical axion bounds diminished by screening effects, Phys. Rev. D 33, 897 (1986).
- [24] G. G. Raffelt, Plasmon decay into low-mass bosons in stars, Phys. Rev. D 37, 1356 (1988).
- [25] A. Ayala, I. Domínguez, M. Giannotti, A. Mirizzi, and O. Straniero, Revisiting the Bound on Axion-Photon Coupling from Globular Clusters, Phys. Rev. Lett. 113, 191302 (2014).
- [26] G. G. Raffelt, Astrophysical axion bounds, Lect. Notes Phys. 741, 51 (2008).

- [27] M. Pospelov, A. Ritz, and M. Voloshin, Bosonic super-WIMPs as keV-scale dark matter, Phys. Rev. D 78, 115012 (2008).
- [28] P. Gondolo and G. G. Raffelt, Solar neutrino limit on axions and keV-mass bosons, Phys. Rev. D **79**, 107301 (2009).
- [29] A. V. Derbin, A. S. Kayunov, V. V. Muratova, D. A. Semenov, and E. V. Unzhakov, Constraints on the axion-electron coupling for solar axions produced by a Compton process and Bremsstrahlung, Phys. Rev. D **83**, 023505 (2011).
- [30] J. Redondo, Solar axion flux from the axion-electron coupling, J. Cosmol. Astropart. Phys. 12 (2013) 008.
- [31] S. Andriamonje *et al.*, An improved limit on the axion-photon coupling from the CAST experiment, J. Cosmol. Astropart. Phys. 04 (2007) 010.
- [32] J. N. Bahcall and M. H. Pinsonneault, What Do We (Not) Know Theoretically about Solar Neutrino Fluxes?, Phys. Rev. Lett. **92**, 121301 (2004).
- [33] V. Anastassopoulos *et al.*, New CAST limit on the axion-photon interaction, Nat. Phys. **13**, 584 (2017).
- [34] M. Arik *et al.*, New solar axion search using the CERN axion solar telescope with ⁴He filling, Phys. Rev. D **92**, 021101(R) (2015).
- [35] W. Buchmüller and F. Hoogeveen, Coherent production of light scalar or pseudoscalar particles in Bragg scattering, Phys. Lett. B 237, 278 (1990).
- [36] E. A. Paschos and K. Zioutas, A proposal for solar axion detection via Bragg scattering, Phys. Lett. B 323, 367 (1994).
- [37] R. J. Creswick, F. T. Avignone III, H. A. Farach, J. I. Collar, A. O. Gattone, S. Nussinov, and K. Zioutas, Theory for the direct detection of solar axions by coherent Primakoff conversion in germanium detectors, Phys. Lett. B 427, 235 (1998).
- [38] F. T. Avignone III, D. Abriola, R. L. Brodzinski, J. I. Collar, R. J. Creswick, D. E. DiGregorio, H. A. Farach, A. O. Gattone, C. K. Guérard, F. Hasenbalg, H. Huck, H. S. Miley, A. Morales, J. Morales, S. Nussinov, A. Ortiz de Solórzano, J. H. Reeves, J. A. Villar, and K. Zioutas (SOLAX Collaboration), Experimental Search for Solar Axions via Coherent Primakoff Conversion in a Germanium Spectrometer, Phys. Rev. Lett. 81, 5068 (1998).
- [39] R. Bernabei *et al.*, Search for solar axions by Primakoff effect in NaI crystals, Phys. Lett. B **515**, 6 (2001).
- [40] A. Morales *et al.*, Particle dark matter and solar axion searches with a small germanium detector at the Canfranc underground laboratory, Astropart. Phys. **16**, 325 (2002).
- [41] Z. Ahmed *et al.*, Search for Axions with the CDMS Experiment, Phys. Rev. Lett. **103**, 141802 (2009).
- [42] E. Armengaud *et al.*, Axion searches with the EDELWEISS-II experiment, J. Cosmol. Astropart. Phys. 11 (2013) 067.
- [43] S. Cebrián *et al.*, Prospects of solar axion searches with crystal detectors, Astropart. Phys. **10**, 397 (1999).
- [44] F. T. Avignone III, Unconventional applications of the Ge detector and the axion, J. Phys. **173**, 012015 (2009).
- [45] W. Xu and S. R. Elliott, Solar axion search technique with correlated signals from multiple detectors, Astropart. Phys. 89, 39 (2017).
- [46] J. Heise, The Sanford underground research facility at Homestake, J. Phys. **606**, 012015 (2015).

- [47] N. Abgrall *et al.*, The MAJORANA DEMONSTRATOR neutrinoless double-beta decay experiment, Adv. High Energy Phys. 2014, 365432 (2014).
- [48] S. I. Alvis *et al.* (MAJORANA Collaboration), Search for neutrinoless double- β decay in ⁷⁶Ge with 26 kg yr of exposure from the MAJORANA DEMONSTRATOR, Phys. Rev. C **100**, 025501 (2019).
- [49] N. Abgrall *et al.*, The MAJORANA DEMONSTRATOR readout electronics system, J. Instrum. **17**, T05003 (2022).
- [50] C. E. Aalseth, P. S. Barbeau, J. Colaresi, J. I. Collar, J. Diaz Leon, J. E. Fast, N. E. Fields, T. W. Hossbach, A. Knecht, M. S. Kos, M. G. Marino, H. S. Miley, M. L. Miller, J. L. Orrell, and K. M. Yocum (CoGeNT Collaboration), Co-GeNT: A search for low-mass dark matter using p-type point contact germanium detectors, Phys. Rev. D 88, 012002 (2013).
- [51] C. G. Wiseman, An axion search with the MAJORANA DEM-ONSTRATOR, Ph.D. thesis, University of South Carolina, 2018.
- [52] C. Wiseman, A low energy rare event search with the MAJORANA DEMONSTRATOR, J. Phys. 1468, 012040 (2020).
- [53] I. J. Arnquist *et al.*, Exotic dark matter search with the MAJORANA DEMONSTRATOR, arXiv:2206.10638.
- [54] United States Naval Observatory, Naval observatory vector astrometry software. C edition, version 3.1.
- [55] W. Verkerke and D. Kirkby, The ROOFIT toolkit for data modeling, in *Statistical Problems in Particle Physics*, *Astrophysics and Cosmology* (World Scientific, Singapore, 2006), pp. 186–189.

- [56] R. Brun and F. Rademakers, ROOT: An object oriented data analysis framework, Nucl. Instrum. Methods Phys. Res., Sect. A 389, 81 (1997).
- [57] S. S. Wilks, The large-sample distribution of the likelihood ratio for testing composite hypotheses, Ann. Math. Stat. 9, 60 (1938).
- [58] I. J. Arnquist *et al.*, A search for spontaneous radiation from wavefunction collapse in the MAJORANA DEMONSTRATOR, Phys. Rev. Lett. **129**, 080401 (2022).
- [59] E. Aprile *et al.* (XENON Collaboration), Excess electronic recoil events in XENON1T, Phys. Rev. D **102**, 072004 (2020).
- [60] L. Di Luzio, M. Fedele, M. Giannotti, F. Mescia, and E. Nardi, Solar Axions Cannot Explain the XENON1T Excess, Phys. Rev. Lett. 125, 131804 (2020).
- [61] J.B. Dent, B. Dutta, J.L. Newstead, and A. Thompson, Inverse Primakoff Scattering as a Probe of Solar Axions at Liquid Xenon Direct Detection Experiments, Phys. Rev. Lett. **125**, 131805 (2020).
- [62] C. Gao, J. Liu, L. T. Wang, X. P. Wang, W. Xue, and Y. M. Zhong, Reexamining the Solar Axion Explanation for the XENON1T Excess, Phys. Rev. Lett. 125, 131806 (2020).
- [63] M. Arik et al., Search for Sub-eV Mass Solar Axions by the CERN Solar Telescope with ³He Buffer Gas, Phys. Rev. Lett. 107, 261302 (2011).
- [64] N. Abgrall *et al.* (LEGEND Collaboration), LEGEND-1000 preconceptual design report, arXiv:2107.11462.